

Characterising the FY-3A Microwave Temperature Sounder Using the ECMWF Model

Qifeng Lu ¹, W. Bell, P. Bauer, N. Bormann
and C. Peubey

Research Department

¹ National Satellite Meteorological Center / China Meteorological Administration (NSMC/CMA)

Submitted to the AMS Journal of Atmospheric and Oceanic Technology,
October 2010

February 2011

This paper has not been published and should be regarded as an Internal Report from ECMWF.

Permission to quote from it should be obtained from the ECMWF.



European Centre for Medium-Range Weather Forecasts
Europäisches Zentrum für mittelfristige Wettervorhersage
Centre européen pour les prévisions météorologiques à moyen terme

Series: ECMWF Technical Memoranda

A full list of ECMWF Publications can be found on our web site under:

<http://www.ecmwf.int/publications/>

Contact: library@ecmwf.int

©Copyright 2011

European Centre for Medium-Range Weather Forecasts
Shinfield Park, Reading, RG2 9AX, England

Literary and scientific copyrights belong to ECMWF and are reserved in all countries. This publication is not to be reprinted or translated in whole or in part without the written permission of the Director-General. Appropriate non-commercial use will normally be granted under the condition that reference is made to ECMWF.

The information within this publication is given in good faith and considered to be true, but ECMWF accepts no liability for error, omission and for loss or damage arising from its use.

Abstract

China's FY-3A, launched in May 2008, is the first in a series of seven polar orbiting meteorological satellites planned for the next decade by China. The FY-3 series is set to become an important data source for Numerical Weather Prediction (NWP), reanalysis and climate science. FY-3A is equipped with a microwave temperature sounding instrument (MWTS). This study reports an assessment of the MWTS instrument using the ECMWF NWP model, radiative transfer modelling and comparisons with equivalent observations from the Advanced Microwave Sounding Unit-A (AMSU-A). The study suggests the MWTS instrument is affected by biases related to large shifts, or errors, in the frequency of the channel passbands as well as radiometer non-linearity. The passband shifts, relative to pre-launch measurements, are 55 MHz, 39 MHz and 33 MHz for channels 2-4 respectively. Relative to the design specification the shifts are 60 MHz, 80 MHz and 83 MHz with uncertainties of ± 2.5 MHz. The radiometer non-linearity results in a positive bias in measured brightness temperatures and is manifested as a quadratic function of measured scene temperatures. By correcting for both of these effects the quality of the MWTS data is improved significantly, with the standard deviations of (observed minus simulated) differences based on short range forecast fields reduced by 30-50% relative to simulations using pre-launch measurements of the passband, to values close to those observed for AMSU-A equivalent channels. The new methodology could be applied to other microwave temperature sounding instruments and illustrates the value of NWP fields for the on-orbit characterisation of satellite sensors.

1 Introduction

China's FY-3A, launched in May 2008, is the first in a series of seven meteorological satellites due to be launched in the period leading up to 2020 by China's Meteorological Administration. The FY-3A payload includes four instruments of particular interest for Numerical Weather Prediction (NWP) and climate science: microwave temperature and humidity sounders; a microwave imager; and an infrared sounder. This study is concerned with the on-orbit performance of the FY-3A microwave temperature sounder (MWTS), the characteristics of which are summarised in Table 1. The MWTS is a cross-track scanning radiometer with a swath width of 2250 km, a nadir footprint size of 62 km and 15 fields of view per scan line. FY-3B, launched in November 2010, also carries an MWTS instrument.

MWTS features four channels which are illustrated in Figure 1. The weighting functions for the sounding channels (2-4) are shown in Figure 2, together with typical mean temperature profiles for different latitude bands. The remaining five platforms (FY-3C - FY-3G) will carry a more advanced microwave sounder with 13 channels, similar in specification to the Advanced Microwave Sounding Unit-A (AMSU-A) (Goodrum et al. (2000)) carried on the NOAA-15 to NOAA-19 platforms, as well as NASA's Aqua platform and EUMETSAT's MetOp-A satellite. MWTS is similar, but not identical, in specification to

Table 1: FY-3A MWTS channel characteristics.

Channel no. (equiv AMSUA)	Frequency / GHz (design)	Bandwidth / MHz	NE Δ T (pre-launch) / K
1 (3)	50.3	180	0.5
2 (5)	53.596 \pm 0.115	2 \times 170	0.4
3 (7)	54.94	400	0.4
4 (9)	57.29	330	0.4

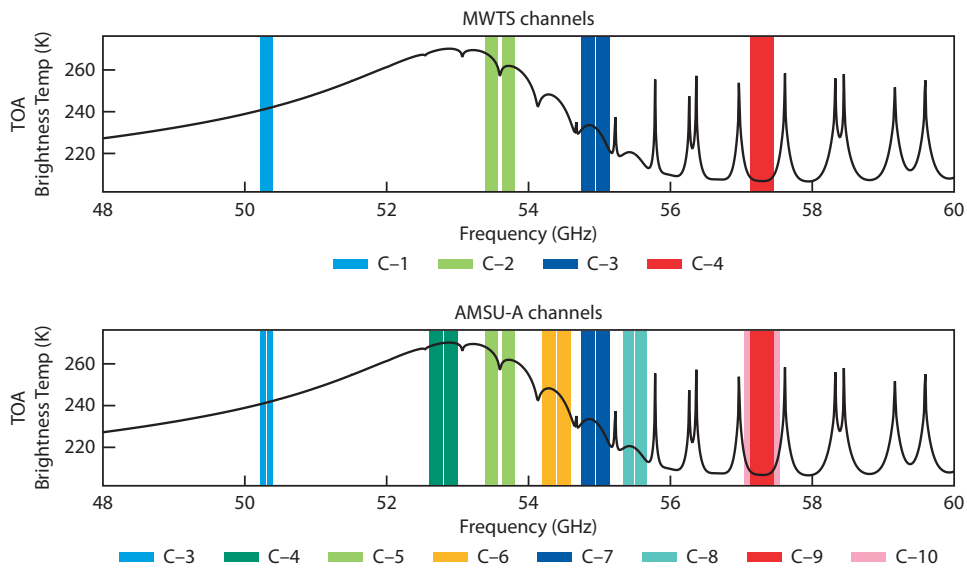


Figure 1: Passbands for the four channels of the FY-3A Microwave Temperature Sounder (upper plot) and AMSU-A channels 3-10 (lower plot). Also shown is a simulation of top-of-atmosphere brightness temperatures (in Kelvin) for a typical tropical atmospheric profile.

the Microwave Sounding Units (MSUs) that were carried on board the NOAA TIROS-N Polar Orbiting Environmental System (POES) series TIROS-N - NOAA-14. Although initial prototype designs for the MWTS had passbands equivalent to MSU (Zhang (2002)), the channel passbands of the FY-3A flight model (Dong et al. (2009)) are identical to the equivalent AMSU-A channels to give continuity with existing NOAA operational instruments.

As a preparatory mission it is important that any instrument related biases in the data are characterised, in order that these biases can be corrected for the FY-3A MWTS and subsequent sensors, and can be dealt with appropriately in NWP data assimilation systems. This study presents evidence of two distinct biases in the MWTS measurements, based on comparisons with ECMWF model fields and with equivalent AMSU-A observations.

Until the recent advent of advanced IR sounding instruments, microwave temperature sounding data from high performance radiometers was the single most important satellite data type in NWP data assimilation systems (English et al. (2004)). Microwave temperature sounding data, by providing accurate information for the analysis of mass fields, is still a key component of NWP data assimilation systems. Recently developed advanced diagnostic tools have confirmed the continuing importance of microwave sounding data in NWP data assimilation systems (Cardinali (2009)).

In today's variational assimilation systems, radiance measurements are routinely compared with NWP model fields mapped to brightness temperatures using radiative transfer modelling. Generally, differences will be non-zero and will comprise large scale slowly varying *systematic* biases, including radiative transfer modelling errors, as well as more small scale *day-to-day* features resulting from local errors in the forecast model fields, in addition to a purely *random* component from the instrument noise. In NWP assimilation systems it is crucial that the stationary, or *quasi-stationary*, components of such biases (which may result from forecast model error, radiative transfer model error, or measurement error) are eliminated prior to assimilation, leaving only the errors in the model fields to be corrected. At ECMWF this is achieved using a variational bias correction scheme (Auligné et al. (2007), Dee (2005)) in which

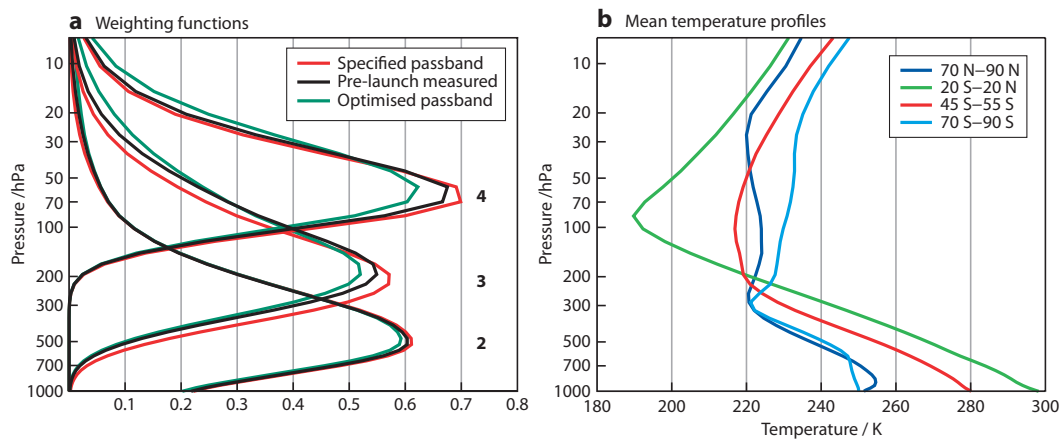


Figure 2: (a) Weighting functions for MWTS channels 2, 3 and 4, based on design specification, pre-launch measurements and optimised estimates of the passband centre frequencies. (b) The mean temperature profiles for the latitude bands indicated (for 17th September 2008), from which the latitudinal dependence of the brightness temperature errors resulting from a (passband shift induced) vertical shift in the weighting function may be inferred.

the biases are represented by a relatively simple linear predictor model involving predictors derived from the model state variables and variables related to the observation geometry. The coefficients of this model form part of the *analysis control vector* and are estimated in each analysis cycle. It is important that this predictor model is able to represent the form of the biases observed. If this is not the case, for example due to biases caused by a process which is not accurately represented by the linear predictor model, residual biases can remain in the data which would degrade the accuracy of the analysis.

This is the case in this study where we present evidence that the FY-3A MWTS observations are affected by a shift in the passband centre frequencies (relative to pre-launch measurements) for three of the four MWTS channels, as well as significant radiometer non-linearity. This evidence is based on a comparison of observations with radiances modelled from ECMWF short range forecast fields. The working assumption here is that the ECMWF model fields are sufficiently accurate to detect, partition and quantify these instrument errors.

NWP models have been used in several investigations recently to characterise errors in microwave satellite observations. [Bell et al. \(2008\)](#) used NWP fields to detect and correct for several biases in SSMIS observations, including biases related to reflector emission and warm load calibration anomalies. This study showed that for temperature sounding channels, instrument errors of several tenths of a Kelvin could be detected using NWP model fields. [Geer et al. \(2010\)](#) showed that a bias related to reflector emission could be identified in observations from the Tropical Rainfall Measuring Mission (TRMM) Microwave Imager (TMI). The fidelity of the NWP short range forecast fields results from the large volume of satellite data which determines the analysis used to produce the short range forecasts. Of particular importance, with respect to the accuracy of the temperature fields in the mid-troposphere to lower stratosphere where the MWTS channels have maximum sensitivity, are the observations from: the advanced IR sounders (AIRS and IASI, see [Collard and McNally \(2009\)](#)); six AMSU-A sensors carried on-board NOAA, NASA and MetOp-A platforms; and data from a constellation of six GPSRO instruments ([Healy and Thépaut \(2006\)](#)). Typical bias corrections for the advanced IR sounders for the temperature sounding channels are several tenths of a Kelvin. For the AMSU-A instruments the bias corrections are generally below 1K. The GPSRO observations, assimilated as bending angles, have very small absolute uncertainties and are assimilated without bias correction, thereby anchoring the NWP

system.

Microwave sounding data, from MSU and AMSU, has been used extensively for climate studies aimed at estimating temperature trends in the troposphere and lower stratosphere (see [Karl et al. \(2006\)](#) and references therein). As part of efforts to reconcile differences between trends derived by independent researchers much effort has been focused on characterising accurately the non-linear response of microwave radiometers to measured radiances. Approaches based on a careful analysis of pre-launch data ([Mo et al. \(2001\)](#), [Grody et al. \(2004\)](#)) as well as approaches which use satellite co-locations in the polar regions have been reported ([Zou et al. \(2006\)](#)). The approach presented here complements these established techniques in identifying, and correcting, two important instrument biases.

Regarding the problems associated with shifts in the centre frequencies of passbands, a recent study (C. Peubey, *pers. comm.*) has concluded that measurable degradations in NWP forecast quality can result from uncorrected passband shifts of 1.5 MHz or larger.

In this study we report a new approach to diagnosing, and correcting, passband shifts and radiometer non-linearity using NWP model fields. This approach has been developed specifically for FY-3A MWTS, but is of general applicability to other microwave temperature sounders. In Section 2 we describe the initial detection of the problem, through a comparison of the MWTS observations with AMSU-A observations, and some initial simulations. A sensitivity study which examined other possible sources (model bias, RT model bias and a range of instrument calibration errors) of the biases detected in the MWTS observations is described in Section 3 which concludes that the most likely causes of the biases are non-linearity and passband shift. In Section 4 we describe the approach used to optimise our estimate of the new instrument parameters. Finally, in Section 5, we demonstrate the improvement in data quality through an inspection and analysis of first guess departure fields, prior to variational bias correction.

2 Comparisons with AMSU-A and Initial Simulations

MWTS data was obtained directly from China's Meteorological Administration. Limited information is available on the details of the pre-processing software but it is known that an antenna pattern correction is performed and calibration data is averaged over seven consecutive scan lines to reduce calibration errors. No non-linearity corrections nor corrections for spacecraft contamination were made in the version of the data used here.

A comparison of MWTS observed brightness temperatures with equivalent MetOp-A AMSU-A observations gives some indication of possible biases in the MWTS observations. Figure 3 shows the measured brightness temperatures for a 12 hour period during 17th September 2008 for both MWTS and the equivalent MetOp-A AMSU-A observations.

MetOp-A (equatorial crossing time 09:30) is in a very similar orbit plane to FY-3A (ascending node equatorial crossing time 10:05) and hence both MWTS and AMSU-A show very similar coverage. From an inspection of the histograms of brightness temperatures it is evident that MWTS brightness temperatures, at the peaks in the histograms, are shifted by $\sim(1-2)$ K for channels 2 and 3, and by 2-3K for channel 4, relative to the AMSU-A observations. The shift is most evident for channels 2-4 as the dynamic range in measured brightness temperatures is relatively small (at 40-60K) compared with the larger dynamical range for channel 1 (~ 140 K, not shown here) which has a significant contribution to the measured radiance from clouds and the surface. From Figure 1 it is seen that these offsets are consistent with positive shifts in band centre frequencies: positive shifts in passband centre frequency cause negative shifts in brightness temperature for channels 2 and 3, and a positive shift for channel 4. At this stage though,

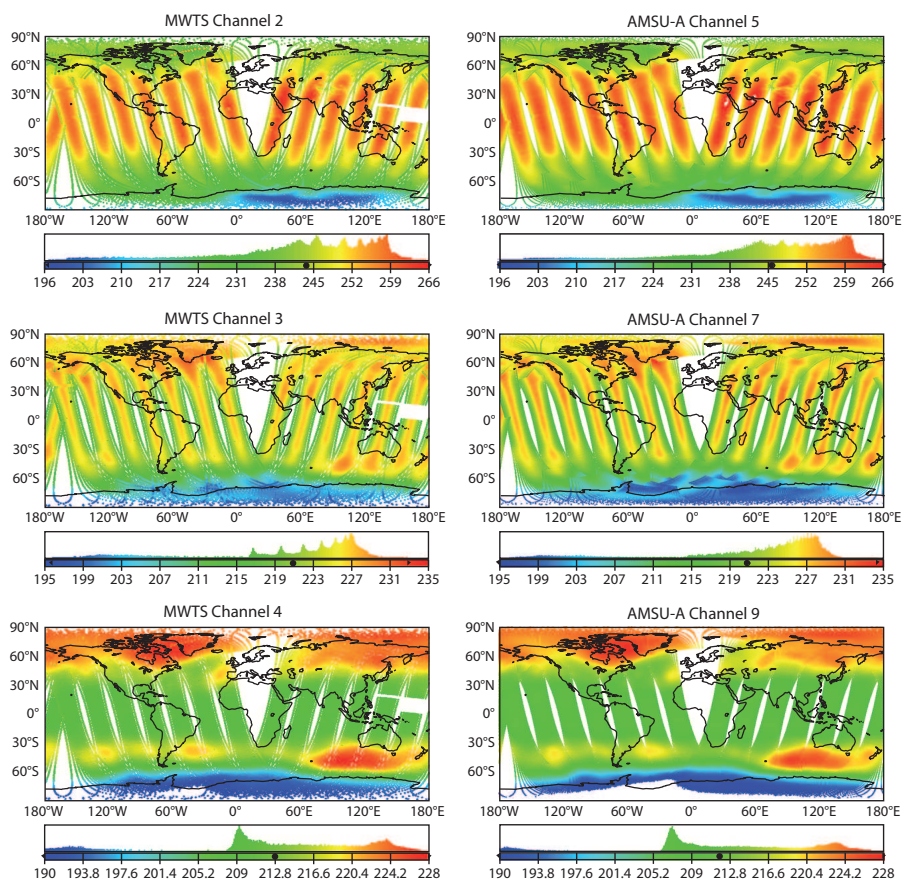


Figure 3: Observed brightness temperatures for FY3-A MWTS and the equivalent MetOp-A AMSU-A channels. The left column shows the observed brightness temperatures for the FY3-A MWTS, the right column shows brightness temperatures for the equivalent MetOp-A AMSU-A channels (for the 12 hour cycle at 00Z on 17th September 2008). The spot at the base of the histograms indicates the mean brightness temperature for each plot.

there are other conceivable causes of this bias which could alias into an *apparent* passband shift error. For channel 4, the shift of +2K is most evident for the primary peak in the histogram, associated with observations in the tropics (at ~ 209 K). There is less evidence of a shift in the secondary maximum (at ~ 224 K) associated with measurements in the northern polar latitudes and an area of the Southern Ocean to the south of Australia.

As an initial step in understanding these biases simulations of the expected brightness temperature error resulting from passband shift were carried out. The simulations used a line-by-line (LbL) radiative transfer model, based on the *Millimetre Wave Propagation Model* of Liebe et al. (1993) (see also Liebe (1989) and Liebe et al. (1992)), hereafter referred to as MPM92, to simulate brightness temperatures for specified levels of passband shift. Initially, a climatological set of atmospheric profiles was used to assess the expected latitudinal dependence of the passband shift induced errors. The consistency of these error estimates with those expected from passband shifts of around 80 MHz (relative to design specification) was sufficient to warrant further investigation of the passband shift hypothesis.

The mechanism which results in this form of error is clear from Figure 1 which shows that passband shifts result in the radiometer sampling different parts of the O_2 spectrum associated with different optical depths. This causes a displacement of the weighting function of the channel (see Figure 2) which in turn

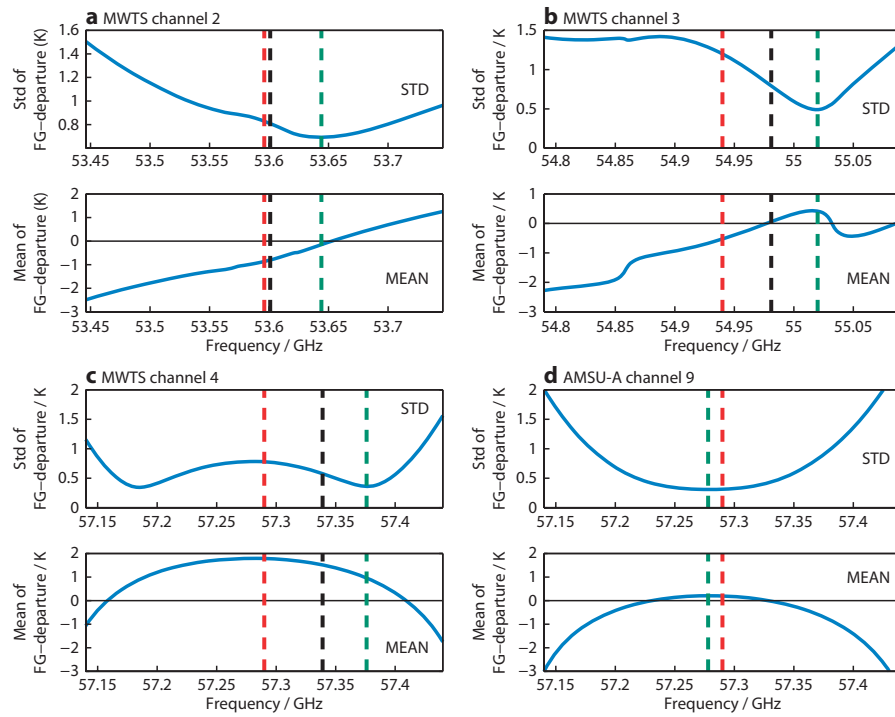


Figure 4: The variation of standard deviation (top) and mean (bottom) of departures (observation minus model equivalent brightness temperatures) with passband shift for MWTS channels 2 (a), 3 (b), 4 (c) and AMSU-A channel 9 (d). The dashed red line shows the design specified passband centre, the black dashed line shows the passband based on pre-launch measurements and the green dotted line shows the frequency corresponding to the minimum in the first guess departures.

results in the radiometer sampling higher or lower parts of the atmosphere. Depending on the local lapse rate in the region of the weighting function peak the shift in the brightness temperature can be positive or negative. For example, for positive shifts in passband frequency for channel 4, the resulting upward shift in the weighting function results in positive shifts in measured brightness temperatures in the tropics where the lapse rate is strongly positive (~ 3 K/km) at the weighting function peak, but relatively small shifts in the northern polar latitudes where the lapse rate is near zero. This type of error is therefore a function of local lapse rate, and not measured brightness temperature, which is the case for radiometer non-linearity error (see Section 3.4 below)

To further investigate the possible passband shift additional line-by-line modelling was conducted to assess the sensitivity of the (observation - model) fit for various passband shifts. Model geophysical fields (temperature and water vapour) were mapped to brightness temperatures for an ensemble of 15000 observations, assuming passband centre frequency shifts in the range ± 150 MHz. Standard deviation and mean differences (observation minus simulation) were generated. The results are shown in Figure 4.

Two points are notable from this figure: firstly, the fit of model fields to the observed brightness temperatures is improved by assuming significant passband shifts for channels 2-4. These shifts halve the standard deviations of (obs-simulation) differences for channels 2-4 relative to those for the un-shifted passbands, based on design specified passbands. There are also significant improvements over simulations using passbands based on pre-launch measurements. Secondly, the position of the minimum in the standard deviation curves corresponds to a reduction in the magnitude of the mean difference between the observations and simulation, *ie* both the magnitude and the structure of the (observation-simulation)

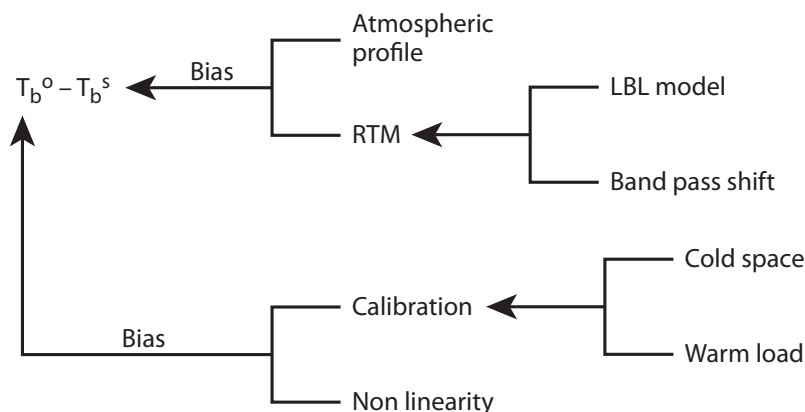


Figure 5: Schematic of error terms considered in the sensitivity study, affecting the departures (observed minus simulated brightness temperatures), $T_b^o - T_b^s$ through the simulation (T_b^s), or directly affecting the observed values (T_b^o).

differences are improved by assuming a passband shift of ~ 40 - 80 MHz. The biases remaining for channel 3 (+0.25K) and channel 4 (+1K) are still non-zero and these are investigated further in Section 3.4 below.

As a check of this approach, a similar analysis was carried out for MetOp-A AMSU-A channel 9, the results of which are shown in Figure 4d. AMSU-A channel 9 does not show a double minimum structure, although a residual bias of 0.2K remains in simulations assuming the nominal designed passband specification.

3 Sensitivity Study

Figure 4 gives a strong indication that passband centre frequency shift accounts for a significant fraction of the variance in the uncorrected observation minus simulation differences (first guess departures). In order to further test this hypothesis a sensitivity analysis was carried out to assess whether other errors, either in the forecast model fields, in the radiative transfer model, or related to the instrument could be manifested as *apparent* passband shift errors. Specifically, we assessed whether a range of errors would be manifested as a double minimum in the plots of the type shown in Figure 4 for MWTS channel 4. The other possible sources of error are summarised schematically in Figure 5.

These errors can affect either the geophysical fields themselves, the mapping of these fields to brightness temperatures, or the observed values of brightness temperature. All of these errors can in principle contribute to the observed biases between observed and simulated brightness temperatures. The sensitivity analysis involved proposing hypothetical errors in model fields, RT model and in the instrument, adding these to the (obs-simulated) fields for AMSU-A channel 9 and assessing the variation of the standard deviation of the differences as a function of assumed passband shift. Here the assumption is that the AMSU-A observations are free of significant errors related to passband shift. The specific form and magnitude of the errors studied is described in Sections 3.1 - 3.4 below.

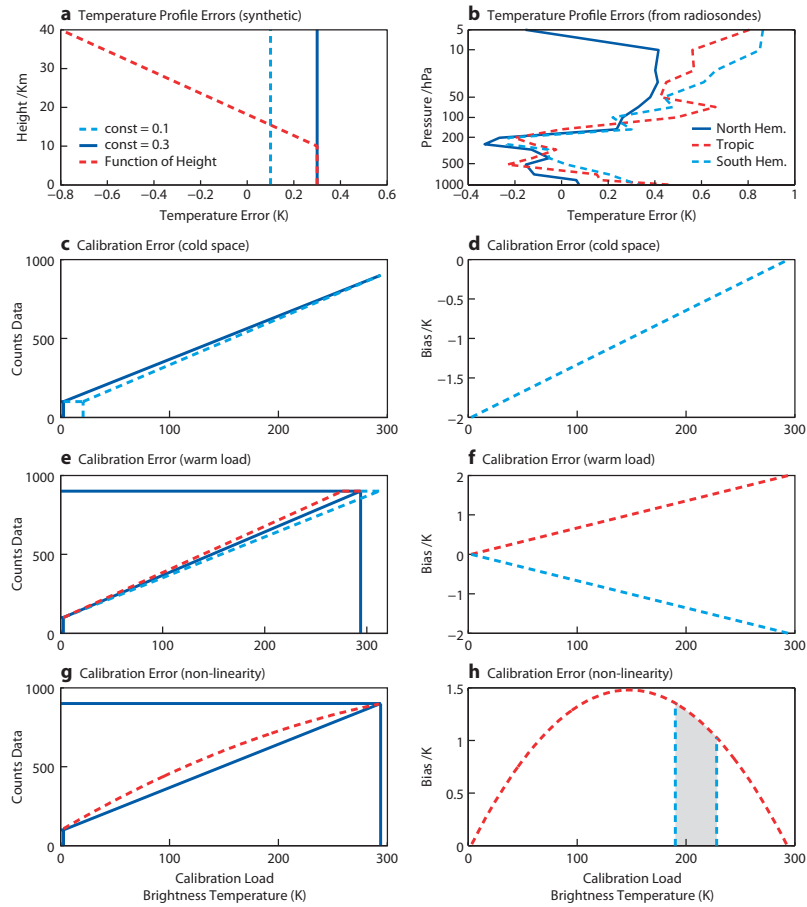


Figure 6: Illustration of the errors considered in the sensitivity study. (a) and (b) show the temperature errors introduced in the model profile, either synthetic or based on radiosonde mean departures respectively. (c) and (d) illustrate the errors expected to result from an error in the cold space measurement. (e) and (f) illustrate the errors expected from a warm load calibration error, with the target temperature assumed erroneously cold and warm. (g) and (h) illustrate the effect of radiometer non-linearity, approximated by a quadratic function. The dynamic range of brightness temperatures MWTS channel 4 is indicated in the shaded area of panel (h). The dashed lines in panels c-h illustrate the form of the true calibration curve, in contrast to the solid lines which show the assumed curve which neglects specific errors.

3.1 Forecast model temperature errors

Errors in the temperature fields themselves will directly influence the fit of model to observations. Several plausible forms of forecast model temperature error were tested. Firstly it could be assumed that differences between model temperatures and radiosonde measurements give an estimate of the true model error. The assumption here is that radiosonde measurements, taken over sufficiently large ensembles, have negligible systematic errors. Statistics on radiosonde fit to model temperatures are readily available and are shown in Figure 6b. Tropospheric biases are generally below 0.5K and are largest at the surface in both the Southern Hemisphere and Tropics. In the lower stratosphere the biases are generally $< 0.8\text{K}$, and significantly smaller in the Northern Hemisphere. As a second approach global errors of 0.1K and 0.3K were assumed (see Figure 6a).

Finally, an error of 0.3K in the troposphere, decreasing monotonically above 10 km to -0.8K at 40 km

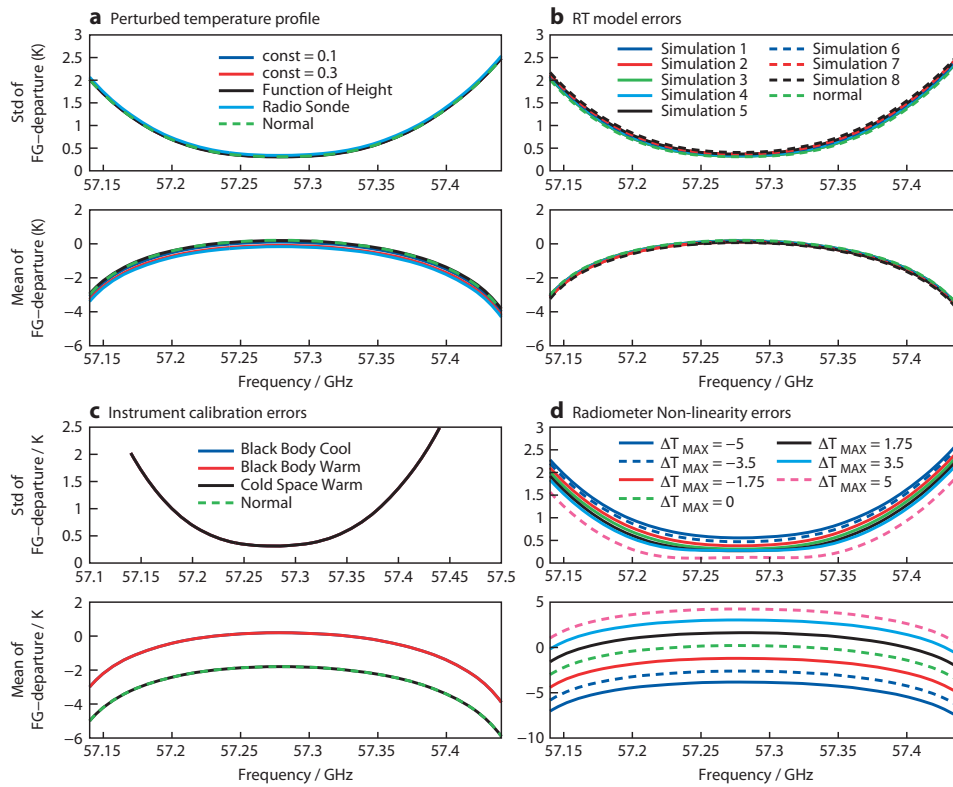


Figure 7: The results of the sensitivity study showing how errors in (a) forecast model temperature profile; (b) radiative transfer model (based on simulations using the scaling factors given in Table 2; (c) instrument calibration and (d) radiometer non-linearity are manifested in the plot of standard deviation (top panels) and mean (bottom panels) of first guess departures versus passband shift. In panel d the magenta dashed line corresponding to a ΔT_{MAX} of 5 has been displaced down by 0.2K to illustrate that a shallow double minimum for this channel appears for very large non-linearities.

was assumed. The envelope of standard deviations of the resulting first guess departures is shown in Figure 7a. None of these hypothetical errors are able to project onto the double minimum feature in the plot of standard deviations of departures for MWTS-4 versus assumed passband shift. Of course these hypothetical errors have very specific forms, and the results here do not conclusively prove the general point that model temperature errors cannot to be manifested as a passband shift type error, but the point is demonstrated that simple model errors do not easily explain the form of the biases. The absence of similar patterns in the first guess departure fields for AMSU-A is a stronger indication that model error is not the likely cause of the biases.

3.2 Radiative transfer model errors

In the *MPM92* model (Liebe (1989), Liebe et al. (1992)) the emission along the observed atmospheric path is derived from the complex refractivity (N_D , in ppm) for dry air which is given by :

$$N_D = N_d + \sum_k S_k F_k + N_n \quad (1)$$

Table 2: Scaling factors for the sensitivity study investigating errors in the line-by-line radiative transfer model (a_1 and a_3 scaling factors).

parameter—simulation	1	2	3	4	5	6	7	8
a_1	1.00	1.00	1.02	1.02	1.02	1.05	1.05	1.05
a_3	1.02	1.05	1.00	1.02	1.05	1.00	1.02	1.05

The second term on the right hand side of equation 1 describes the resonant absorption from discrete rotational transition lines, each described by a line strength (S_k) and a line shape function (F_k). N_d is a non-dispersive term and N_n is the O₂ non-resonant term. For observations in the 50-60 GHz part of the microwave spectrum the main contribution to N_D results from 44 discrete O₂ spectral lines. S_k and F_k are given by:

$$S_k = (a_1/v_k)p_d\theta^3 \exp(a_2(1-\theta)) \quad (2)$$

$$F_k(\nu) = \nu \left[\frac{1 - i\delta_k}{\nu_k - \nu - i\gamma_k} - \frac{1 + i\delta_k}{\nu_k + \nu + i\gamma_k} \right] \quad (3)$$

Where θ is a reciprocal temperature variable ($\theta = 300/T$) with temperature T in Kelvin. p_d is the partial pressure for dry air. The original Van-Vleck Weisskopf line shape function (Van-Vleck and Weisskopf (1945)), which is a function of frequency (ν) with parameters associated with the line centre frequency (ν_k) and line width (γ_k), has been modified by Rosenkranz (1993) to include line overlap effects by additionally including the parameter δ_k . In MPM92 the linewidth (γ , in GHz) and overlap (δ) parameters for pressure broadened O₂ lines in air are:

$$\gamma_k = a_3 \times 10^{-3} (p_d\theta^{a_4} + e\theta) \quad (4)$$

$$\delta_k = (a_5 + a_6\theta)p\theta^{0.8} \quad (5)$$

Where e is the partial pressure of water vapour (in mbar).

The parameters a_i are specified in the MPM92 model based on an analysis of laboratory spectra (Liebe et al. (1993)). The uncertainties associated with the parameters a_i are discussed in Liebe et al. (1993) where it is suggested that the measurement uncertainties are $\sim 2\%$ for line strength and $\sim 5\%$ for line width. In this part of the study the most significant parameters (a_1 and a_3) governing the computation of absorption cross sections were perturbed by a maximum of 5% as indicated in Table 2.

The results shown in Figure 7b demonstrate that errors of this type and magnitude do not project onto an apparent passband shift error. This is at first sight surprising as a line strength error would be expected to be manifested as an optical depth error similar to that caused by passband shift. The likely explanation is that much larger errors in the line parameters, not supported by the spectroscopic measurements reported in Liebe et al. (1993), would be required to cause the observed biases.

It is noteworthy that the absence of similar biases in the equivalent AMSU-A observations *independently* reduces the likelihood that the observed MWTS biases are related to model error or radiative transfer model error as these errors are common to both MWTS and AMSU-A.

3.3 Instrument calibration errors

Several types of instrument error related to the radiometric calibration of the instrument can be envisaged. These are illustrated schematically in Figure 6. Figures 6c and 6d illustrate the consequences of a calibration error affecting the cold space calibration point, for example through field-of-view contamination by some part of the spacecraft. The result of such effects is that for a given scene count, the derived scene temperature would be converted to an erroneously low brightness temperature, the magnitude of the error would increase monotonically as observed temperatures tended towards the temperature of cold space. Of course, for the channels studied here, the range of observed brightness temperatures have a lower limit of 160K.

Figures 6e and 6f illustrate schematically the consequences of a warm load calibration error. This type of error could result from thermal gradients across the the warm calibration load causing a load radiometric temperature warmer (or colder) than the temperature measured by the platinum resistance thermometers embedded in the calibration load. The resulting biases increase monotonically from cold space as scene temperatures increase. The results, shown in Figure 7c, demonstrate that this class of calibration error cannot account for the double minimum structure in MWTS-4.

Figures 6g and 6h show the effect of detector non-linearity. The detector response ($\frac{\partial(\text{counts})}{\partial(T_{sc})}$) is larger at low measured scene temperatures (T_{sc}). At the calibration load temperatures (2.7K and 300K) the error is close to zero, but shows a maximum at the mid-point ($\sim 148\text{K}$). For a channel such as MWTS channel 4, where the range of scene temperatures is 185-240 K, this type of error would be manifested as: (i) a positive bias; and (ii) an increase in the bias towards lower temperatures. A negative bias could be envisaged, but is less likely as it would require the radiometer sensitivity to *increase* with increasing scene radiance rather than the saturation effect normally observed. This bias is quadratic in form, but over a narrow dynamic range could be manifested as an approximately linear variation in the error *versus* scene temperature. The results are shown in Figure 7d. For large non-linearities ($\Delta T_{MAX} = 5\text{ K}$) the standard deviation curves begin to show a double minimum structure, similar to that for MWTS-4. Although such large non-linearities are unlikely to be the cause of the apparent passband shift, the results of the sensitivity study drew our attention to the possibility of radiometer non-linearity contributing to the observed biases.

3.4 Non-linearity errors

The passband shifts derived above (Section 2, Figure 4) were applied to the simulations for MWTS channels 2-4. The residual first guess departures are shown in Figure 8 plotted against measured scene temperature. Prior to the application of an optimised estimate of the passband centre frequencies, the first guess departures show a complex dependency on the scene temperature, consistent with the passband shift error being directly dependent on vertical temperature gradients rather than temperature directly. After applying the more optimal passband parameters, the data collapses onto a clear *near-linear* relationship, consistent with the expected local appearance of a quadratic error term resulting from radiometer non-linearity. Removal of a quadratic error term of magnitude (ΔT_{MAX}) in the range -0.3 to 1.5K results in unbiased data with a much reduced dependency on measured scene temperature, as will be demonstrated in the next section.

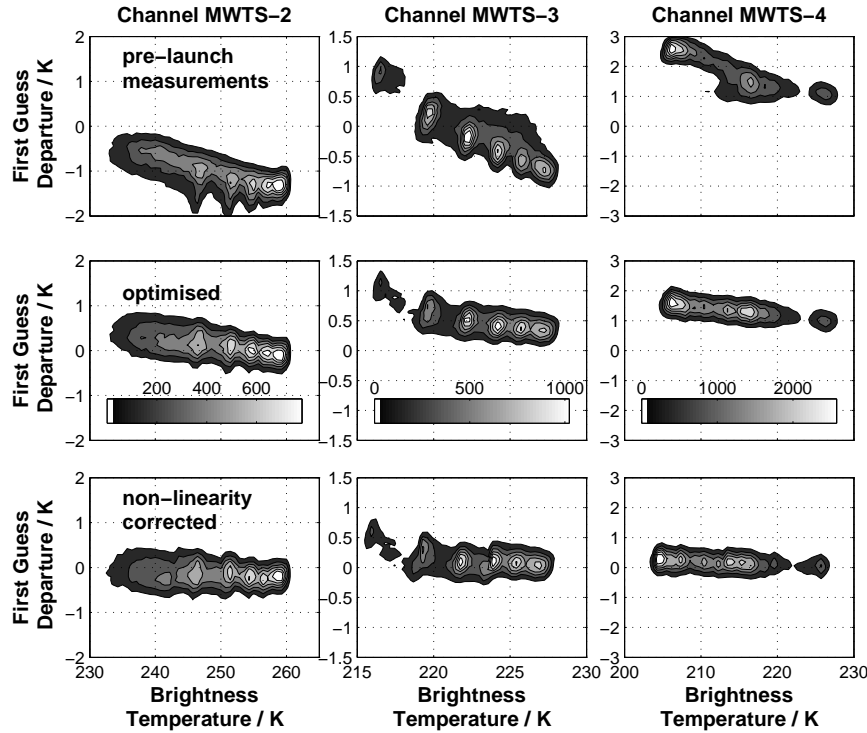


Figure 8: 2D histograms of first guess departures versus scene brightness temperature for (left to right) MWTS channels 2, 3 and 4 for pre-launch measured passbands (top), optimised passbands (middle) and non-linearity corrected data (bottom). The contours are generated from a 50×50 grid over the range of brightness temperatures and first guess departures shown. The number of observations per bin are indicated in colour bars in the middle plots.

4 Optimisation

Following the results described above in Section 3.4 a simple scheme was devised to simultaneously estimate the parameters describing the passband shift ($\Delta\nu_0$) and the non-linearity error (ΔT_{max} , described in the *Appendix*). The scheme involved computing the mean and standard deviation of (observations - simulated observations) from an ensemble of 15000 observations. Simulations were carried out using the MPM92 line-by-line model. Bandwidths for each channel were taken from specified values and this parameter was not varied in the optimisation. Non-linearity errors were computed using a quadratic error (see *Appendix*). This quadratic form was derived assuming errors are zero at calibration points (at temperatures of 2.7K and 294K for the cold space and warm load views respectively), and is fully characterised by a single parameter (ΔT_{max}) which is the maximum brightness temperature error, expected at $T_{sc} = 0.5(T_{cold} + T_{warm})$. The computed mean ($m(\Delta\nu_0, \Delta T_{max})$) and standard deviation ($s(\Delta\nu_0, \Delta T_{max})$) of the departures are shown in Figure 9.

As both factors are important in constraining the optimal estimate of the instrument parameters these were combined in an empirical penalty function, $J(\Delta\nu_0, \Delta T_{max})$:

$$J(\Delta\nu_0, \Delta T_{max}) = \frac{m(\Delta\nu_0, \Delta T_{max})^2}{\sigma_m^2} + \frac{s(\Delta\nu_0, \Delta T_{max})^2}{\sigma_s^2} \quad (6)$$

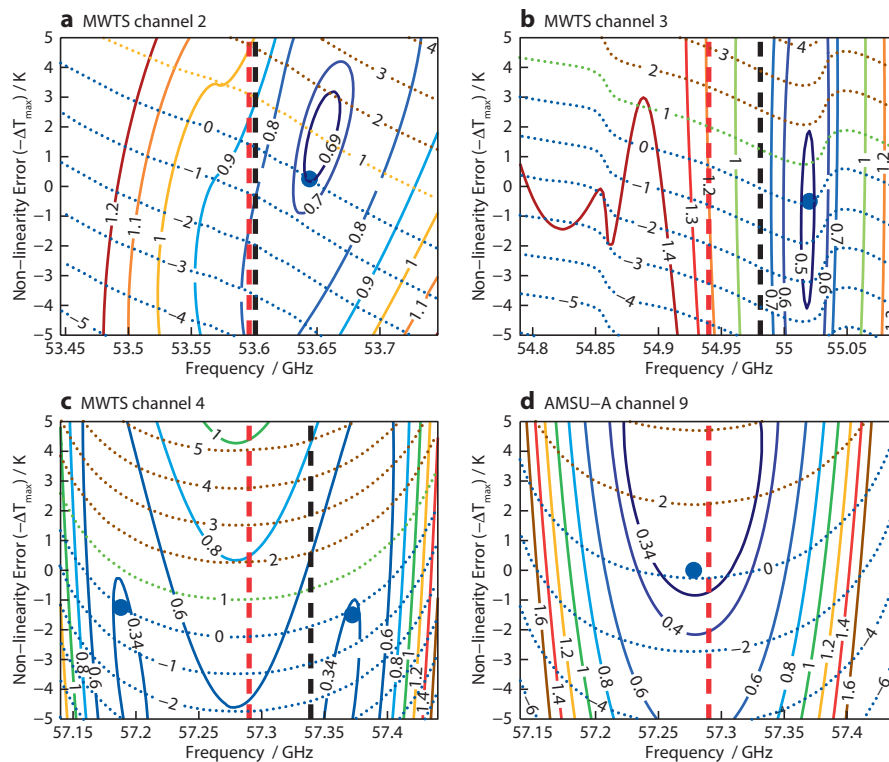


Figure 9: Results of the optimisation for MWTS channels 2-4 (a-c respectively) and (d) AMSU-A channel 9. Each plot shows the standard deviation (solid coloured contours) and mean (dotted coloured contours) of departures against the passband centre frequency (x-axis) and non-linearity parameter (ΔT_{MAX} , y-axis). The position of the design specified passband centre is shown as the red vertical dotted line, the black dotted line shows the pre-launch measurements. The spots indicate the optimised estimates of the passband centre and non-linearity parameter for each channel.

Table 3: Modified MWTS channel characteristics

	MWTS Channel		
	2	3	4
Design passband / GHz	53.596	54.94	57.29
Pre-launch measurement / GHz	53.601	54.981	57.340
Optimised estimate / GHz	53.656	55.020	57.373
Rescaled / GHz	53.633	55.013	57.373
Non-linearity (ΔT_{MAX}) / K	-0.3	0.6	1.5

Where σ_m and σ_s are chosen to represent our estimate, based on an educated guess, of the uncertainties in the expected residual bias and tolerable increase in standard deviation relative to the absolute minimum obtained over the parameter space. These values were chosen to be 0.25K for the uncertainty in the residual bias and 2% of the minimum standard deviation over the parameter space. A tolerable residual bias (before variational bias correction) of 0.25K is in broad agreement with the bias corrections currently applied to other similar radiance observation types in the ECMWF system (*eg* AMSU-A, AIRS and IASI). In addition the uncertainty in the brightness temperature of the black body target used for the instrument end-to-end calibration is around 0.3K at 95 % confidence. Calculations were performed to estimate the variation in the derived instrument parameters for variations in σ_m and σ_s . This showed the estimates to be relatively robust for large changes ($\times 5$) in either parameter. This results from the relatively deep (shallow) minimum in the standard deviations with respect to passband shift (non-linearity). On the other hand the mean difference shows relatively slow (fast) variations with respect to passband shift (non-linearity). The mean and standard deviations of the observed-simulated differences give two independent pieces of information to help estimate the new parameters: the standard deviation yields information about how the new parameters fit the *structure* of the departure fields; whereas the mean gives information about how well the new parameters allow the simulations to fit the overall magnitude of the observed brightness temperature field.

The code was parallelised to run on the ECMWF IBM high performance supercomputer. Simulations took ~ 10 hours for an ensemble of 15000 observations for MWTS channels 2-4. Figure 9 shows contours of mean and standard deviation of the departures *versus* passband shift and non-linearity parameter. The points indicate the position of the minimum in the penalty function defined in Equation 6. The associated values for the new passband and non-linearity parameters are given in Table 3.

In deciding on an optimised set of instrument parameters inter-channel consistency was also a consideration. For channel 4 the double minimum in Figure 9c supports two possible choices of $\Delta\nu_0$ and ΔT_{max} , one associated with negative passband shifts, the other positive. The shifts for channels 2 and 3 are both positive, at +45 MHz and +51 MHz respectively, and this suggests the shift for channel 4 is also likely to be positive. Conceivable physical mechanisms which could explain the shift, for example calibration errors in the pre-launch measurement of the local oscillators (LOs) or on-orbit temperature tuning of the LOs, are most likely to affect all channels similarly.

From Table 3 it can be seen that the passbands for channels 2, 3 and 4 are shifted by +55 MHz, +39 MHz and +33 MHz relative to pre-launch measurements, and by +60 MHz, +80 MHz and +83 MHz relative to design specification respectively. The non-linearities (expressed as ΔT_{max}) are -0.3 K, 0.6 K and 1.5 K respectively.

The uncertainties in the optimised parameters were estimated through an analysis of the reproducibility

of the optimisation. Over 28 independent consecutive 12 hour cycles during February 2010 the standard deviation of the passband shift was 4.6 MHz, 0.66 MHz and 1.57 MHz for channels 2, 3 and 4 respectively. The larger scatter in the optimised parameters for channel 2 results from the contamination of the measured radiances by clouds. The optimised parameters derived from February 2010 were checked using data from a cycle on 17th September 2008 and were found to be stable. In the absence of significant systematic error in these estimates, these reproducibility values would translate to uncertainty estimates below 1 MHz for channels 2-4 (by taking the *standard error of the mean* of the estimates), however the uncertainty is most likely dominated by systematic components. A significant systematic error is associated with the choice of tolerable residual bias. If a tolerable residual bias of 0.25K is assumed, the resulting uncertainty in the estimates of $\Delta\nu_0$ and ΔT_{MAX} can be obtained by projecting this bias, taken along the semi-major axis of the *minima* of Figure 9 onto the y - and x - axes of Figure 9 respectively. The resulting uncertainty estimates, at 95%, are 2.5 MHz in passband shift, and 0.5K in ΔT_{MAX} , however, it should be emphasised that this is a crude estimate and further work is needed to understand all possible systematic contributions to the error in this estimate.

In the later stages of this study, the instrument manufacturer revealed that a likely explanation for the apparent passband shift on-orbit was linked to the resonant cavity used to tune the frequency of the local oscillator. The frequency of the oscillator is governed by the modes of the cavity which are dependent upon the cavity length and refractive index. The change in the refractive index of the medium filling the cavity (*air* for the laboratory based pre-launch measurements and near-vacuum conditions on-orbit) was used to compute new passband centre frequencies which are shown in Table 3 (see *Rescaled* estimates of the passband centre). These shifts are +32 MHz, +32 MHz and +33 MHz for channels 2-4 respectively. These values are in excellent agreement with the optimised estimate provided here for channel 4, less good for channel 3 and well outside our initial estimated error bounds for channel 2. The reason for the poor agreement for channel 2 could be related to an optimistic estimate of the tolerable residual bias and the higher sensitivity of the channel 2 estimate to this assumption, but further work is needed to confirm this. Nevertheless, the study presented here based on NWP fields and radiative transfer modelling has clearly highlighted a problem with the initial specifications.

5 Results and Discussion

The overall effect of the revised instrument parameters is illustrated in Figure 10, which shows the MWTS channel 2-4 first guess departures for passband centre frequencies given by: (a) design specification; (b) pre-launch measurements; and (c) optimised estimates. Figure 10 (d) shows the departures after non-linearity correction (but prior to variational bias correction) and, for comparison, the equivalent AMSU-A first guess departures (e). Figure 10 shows the significant and continuous improvement in first guess departures from simulations using the specified passbands, through the use of pre-launch measurements to optimised estimates of the passband centres and finally the inclusion of an optimised non-linearity correction. The statistics (mean and standard deviation) are summarised in Figure 11. The standard deviations for MWTS channels 2, 3 and 4 are reduced by 37%, 81% and 64% relative to design specifications and by 30%, 52% and 51% relative to pre-launch measurements. Standard deviations for the corrected data are 0.51K, 0.25K and 0.25K, which compare favourably with the equivalent AMSU-A values of 0.56K, 0.36K and 0.29K. Mean biases are reduced to -0.31K, -0.035K and 0.003K, which again compare favourably to AMSU-A equivalents of 0.59K, -0.059K and 0.172K. The systematic biases corrected here were found to be stable and the corrections applied resulted in similar improvements to first guess departures for data obtained 18 months apart.

It is expected that the use of variational bias correction will further reduce the spread in both MWTS and

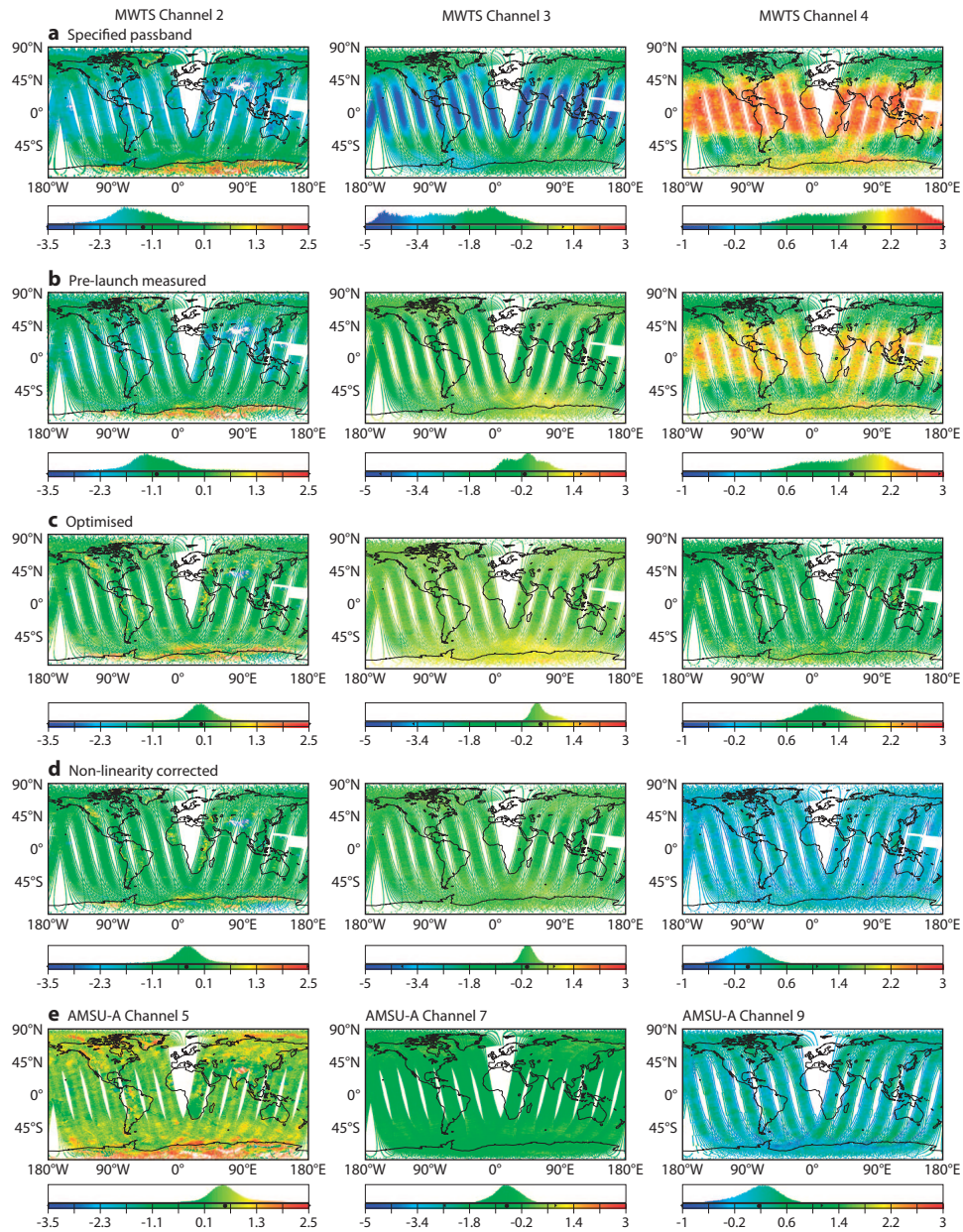


Figure 10: Maps of first guess departures, in Kelvin, for (left to right columns) MWTS channels 2-4 showing departures using (a) design specified passbands; (b) the pre-launch measured passbands; (c) the optimised passbands; (d) after non-linearity correction and (e) the equivalent MetOp-A first guess departure maps. The spots at the base of the histograms indicate the mean first guess departure.

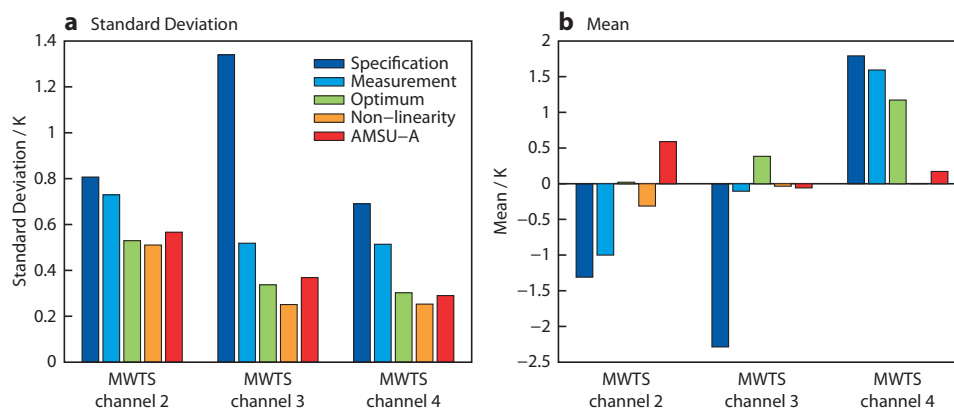


Figure 11: (a) Standard deviations and (b) Means of first guess departures for MWTS channels 2, 3 and 4 for design specified passbands, pre-launch measured passbands, optimised passbands and finally non-linearity corrected passbands. Also shown are the statistics for equivalent MetOp-A AMSU-A channels.

AMSU-A departures due to residual forecast and RT model biases as well as instrument effects. Further reductions of $\sim 30\%$ in the standard deviations for AMSU-A channels 5,7 and 9 are expected, based on previous experience. The *on-orbit* noise performance of the MWTS radiometer was estimated by computing histograms of standard deviations of the observed brightness temperature for small ensembles of observations as described in Bell et al. (2008) (see Figure 12). Also shown for comparison in Figure 12 is an analysis of equivalent channels from NOAA-19 AMSU-A. The MWTS *on-orbit* NE Δ T values (in the range 0.14-0.19K) are significantly lower than the design specification of 0.4K. These NE Δ T values represent the lower limit to the achievable standard deviations for the first guess departures. The estimates for NOAA-19 channels 5,7 and 9 were cross-checked with values derived from on-orbit data over the same period, using the method described in Atkinson and McLellan (1998). The agreement was better than 0.045K for these channels.

For operational purposes the passband shift is best dealt with through an update to the regression coefficients used in fast radiative transfer models. The non-linearity correction is best handled within the ground processing systems, ideally based on accurate pre-launch radiometric measurements. In the short term tests at ECMWF have commenced using the brightness temperature corrections derived here.

Further numerical experiments are required to assess how much further the MWTS standard deviations are reduced prior to assimilation. The effect of the revised passband frequencies on the weighting functions for MWTS channels 2-4 is shown in Figure 2. The new passband specifications result in an upwards displacement of the weighting functions.

In summary the quality of the Level 1B MWTS data has been significantly improved by two physically based corrections to the data: passband shift and radiometer non-linearity. The novel approach presented here illustrates the usefulness of NWP model fields and radiative transfer modelling in characterising satellite sounders *on-orbit*. The methodology has been demonstrated for FY-3A MWTS but is applicable to other microwave temperature sounders, for example subsequent FY-3 sensors, AMSU-A, the Special Sensor Microwave Imager/Sounder (SSMIS) and the Advanced Technology Microwave Sounder (ATMS). The method could be adapted to *operationally* monitor the orbital and long term stability of these instrument parameters.

NWP models should continue to play a role in the calibration and validation of satellite sounding instruments, complementing other established techniques for characterising instrument performance. One

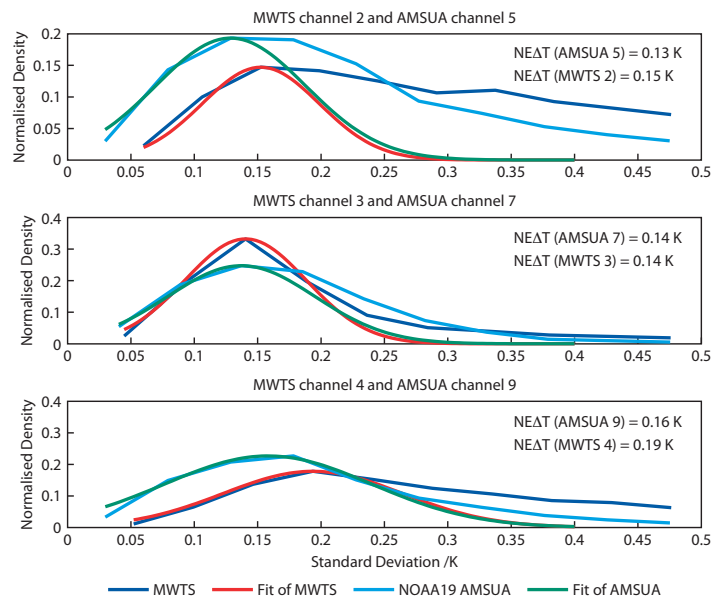


Figure 12: Estimates of $NE\Delta T$ for MWTS channels 2-4 and NOAA-19 AMSU-A channels 5, 7 and 9. Each plot shows the standard deviation for ensembles of clusters (of 6 fields of view) of MWTS/AMSU-A observations. The low standard deviation edge of the curves are fitted to a Gaussian function to estimate the $NE\Delta T$ (indicated).

advantage offered by this type of analysis is that the global nature of the analysis means that most of the dynamic range of measured brightness temperatures and atmospheric variability is probed in each analysis cycle, enabling passband errors and non-linearity errors to be characterised very efficiently.

This study also illustrates the increasing requirement for improved pre-launch calibration of satellite instruments for operational meteorology. It could be argued, based on these results, that this technique alleviates the need for accurate pre-launch measurements, however the widespread application of this type of data for climate research and reanalysis means the data will, in time, be subject to intense scrutiny. This being the case, it is best that this type of analysis is used *in conjunction* with careful pre-launch characterisation (Saunders et al. (1995) and Mo (1996) provide examples of best practise) ideally based on metrologically traceable measurements of the instrument and relevant sub-systems.

Regarding further work, the extension of this technique to other sensors, as well as establishing operational monitoring capabilities have been mentioned above. Uncertainties in the estimate of the passband shift and non-linearity parameters have been discussed but more work could be done to determine more robust uncertainties. Finally, additional work will be carried out to quantify the impact of the revised data on NWP analysis and forecast quality.

Acknowledgements

This study was made possible by support from the EUMETSAT NWP Satellite Application Facility (NW-PSAF) visiting scientist program for Qifeng Lu's visit to ECMWF. The authors would like to thank Tony McNally of ECMWF for arranging this visit. This work was also supported by the bilateral cooperation agreement between ECMWF and the China's Meteorological Administration (CMA) and by the National Natural Science Foundation of China (Grant No. 40705037). The work was also supported by China's

Research and Development Special Fund for Public Welfare Industry (Meteorology GYHY(QX)2007-6-9 and GYHY200906006). Nigel Atkinson at the Met Office kindly provided estimates of NOAA-19 AMSU-A radiometric noise. Rob Hine and Anabel Bowen provided the figures for the memorandum.

Appendix: Parametrising the Non-linearity Correction

This *Appendix* shows that the non-linearity error can be characterised by a single parameter, ΔT_{MAX} , which defines the coefficients in a quadratic approximation for the error.

It is assumed here that the radiometer non-linearity error (ΔT) is well approximated by a quadratic expression in the measured scene temperature (T):

$$\Delta T = c_0 + c_1 T + c_2 T^2 \quad (7)$$

This error is subject to the constraint that the error is zero at the cold space (T_c) and warm load (T_w) temperatures:

$$c_0 + c_1 T_c + c_2 T_c^2 = 0 \quad (8)$$

$$c_0 + c_1 T_w + c_2 T_w^2 = 0 \quad (9)$$

The error can then be defined in terms of a single parameter, ΔT_{MAX} , which represents the maximum amplitude of the error over the range $[T_c, T_w]$. This value for the maximum error, found at $T = \frac{(T_c + T_w)}{2}$, introduces a third equation:

$$c_0 + c_1 \left(\frac{T_c + T_w}{2} \right) + c_2 \left(\frac{T_c + T_w}{2} \right)^2 = \Delta T_{MAX} \quad (10)$$

Equations 8, 9 and 10 can be solved for the coefficients c_0 , c_1 and c_2 to give:

$$c_0 = \frac{-4\Delta T_{MAX} T_c T_w}{(T_c - T_w)(T_c + T_w)} \quad (11)$$

$$c_1 = \frac{\Delta T_{MAX}}{T_c - T_w} \quad (12)$$

$$c_2 = \frac{-4\Delta T_{MAX}}{(T_c - T_w)(T_c + T_w)} \quad (13)$$

This formulation of the non-linearity error was used in the optimisation described in Section 4 and summarised in Figure 9 in order to reduce the degrees of freedom for the optimisation using the *strong* constraint that the error (ΔT) is identically zero at T_c and T_w . For the non-linearity corrections illustrated in Figure 8 the coefficients c_0 , c_1 and c_2 in Equation 7 were allowed to vary independently using a weaker constraint on the value of ΔT at T_c and T_w . This allows the fit to account for radiometric offsets and errors linear in the scene brightness temperature known to affect microwave radiometers. The numerical values for c_0 , c_1 and c_2 are given in Table 4.

This scheme outlined in Equations 7 - 13 is similar, in some respects, to that presented in Zou et al. (2009) for the re-calibration of MSU data in which (following the notation of Zou et al. (2009)) the Earth scene radiance (R) is given by:

Table 4: Coefficients used in the non-linearity corrections

	MWTS Channel		
	2	3	4
a_0	0.079546796	0.070824104	0.000859831
a_1	0.015843045	0.025371222	0.027636840
a_2	-0.000060438557	-0.000107616679	-0.000103839638

$$R = R_L - \delta R + \mu Z \quad (14)$$

Where R_L is the dominant linear response:

$$R_L = R_c + S(C_e - C_c) \quad (15)$$

The non-linear response is given by:

$$Z = S^2(C_e - C_c)(C_e - C_w) \quad (16)$$

Where :

$$S = \frac{(R_w - R_c)}{(C_w - C_c)} \quad (17)$$

and C_e , C_c and C_w are the counts corresponding to the Earth scene, cold space and warm calibration targets respectively. R_c and R_w are the radiances associated with the cold space views and warm target views respectively. δR represents a radiance offset. The non-linear coefficient μ was found to be a function of the MSU instrument temperature. This scheme and that presented in Equations 7 - 13 share the property that the non-linearity error is zero at the calibration points.

References

- Atkinson, N. and S. McLellan, 1998: Initial Evaluation of AMSU-B In-Orbit Data. *SPIE Proceedings: Microwave Remote Sensing of the Atmosphere and Environment, (Beijing 1998)*.
- Auligné, T., A. P. McNally, and D. P. Dee, 2007: Adaptive Bias Correction for Satellite Data in a Numerical Weather Prediction System. *Q. J. R. Met. Soc.*, **133**, 631–642.
- Bell, W., et al., 2008: The Assimilation of SSMIS Radiances in Numerical Weather Prediction Models. *IEEE Transactions on Geoscience and Remote Sensing*, **46**, 884–900.
- Cardinali, C., 2009: Monitoring the observation impact on the short-range forecasts. *Q. J. R. Met. Soc.*, **135**, 239–250.
- Collard, A. D. and A. P. McNally, 2009: The assimilation of Infrared Atmospheric Sounding Interferometer radiances at ECMWF. *Q. J. R. Met. Soc.*, **135**, 1044–1058.

- Dee, D. P., 2005: Bias and Data Assimilation. *Q. J. R. Met. Soc.*, **131**, 3323–3343.
- Dong, C., et al., 2009: An Overview of Chinese New Weather Satellite FY-3A. *Bulletin of The American Meteorological Society*, **90**, 1531–1544.
- English, S. J., R. Saunders, B. Candy, M. Forsythe, and A. Collard, 2004: Met Office Satellite Data Observing System Experiments. *3rd WMO Workshop on the Impact of Various Observing Systems in Numerical Weather Prediction*, Alpbach, Austria, WMO.
- Geer, A. J., P. Bauer, and N. Bormann, 2010: Solar biases in microwave imager observations assimilated at ECMWF. *IEEE Trans. Geosci. Remote Sens.*, **48**, 2660 – 2669.
- Goodrum, G., K. B. Kidwell, and W. Winston, 2000: NOAA KLM Users Guide. [Available online at <http://www2.ncdc.noaa.gov/docs/klm>].
- Grody, N. C., K. Vinnikov, M. D. Goldberg, J. T. Sullivan, and J. D. Tarpley, 2004: Calibration of Multi-satellite Observations for Climatic Studies: Microwave Sounding Unit (MSU). *Journal of Geophysical Research*, **109**, D24 104.
- Healy, S. and J.-N. Thépaut, 2006: Assimilation experiments with CHAMP GPS radio occultation measurements. *Q. J. R. Met. Soc.*, **132**, 605–623.
- Karl, T. R., S. J. Hassol, C. D. Miller, and W. L. Murray, 2006: Temperature Trends in the Lower Atmosphere: Steps for Understanding and Reconciling Differences. US Climate Change Science Program: Synthesis and Assessment Product 1.1 [Available online at <http://www.climate-science.gov/Library/sap/sap1-1/finalreport/default.htm>].
- Liebe, H., 1989: MPM - An Atmospheric Millimeter-Wave Propagation Model. *International Journal of Infrared and Millimeter Waves*, **10**, 631–650.
- Liebe, H., G. Hufford, and M. Cotton, 1993: Propagation modeling of moist air and suspended water/ice particles at frequencies below 1000 GHz. *AGARD 52nd Specialists' Meeting of the Electromagnetic Wave Propagation Panel, Palma de Mallorca, Spain*.
- Liebe, H. J., Rosenkranz, P.W., and G. Hufford, 1992: Atmospheric 60-GHz Oxygen Spectrum: New Laboratory Measurements and Line Parameters. *Journal of Quantitative Spectroscopy and Radiative Transfer*, **48**, 629–643.
- Mo, T., 1996: Prelaunch calibration of the advanced microwave sounding unit-A for NOAA-K. *IEEE Transactions on Microwave Theory and Techniques*, **44 (8)**, 1460.
- Mo, T., M. D. Goldberg, D. S. Crosby, and Z. Cheng, 2001: Recalibration of the NOAA Microwave Sounding Unit. *Journal of Geophysical Research*, **106**, 10,145–10,150.
- Rosenkranz, P. W., 1993: Absorption of Microwaves by Atmospheric Gases. *Atmospheric Remote Sensing by Microwave Radiometry, Chapter 2*, Ed. M. A. Janssen, Wiley and Sons, (ISBN 0 471 62891 3, 37–90).
- Saunders, R., T. Hewison, S. Stringer, and N. Atkinson, 1995: The radiometric characterization of AMSU-B. *IEEE Transactions on Microwave Theory and Techniques*, **43 (4)**, 760–771.
- Van-Vleck, J. H. and V. F. Weisskopf, 1945: On the Shape of Collision Broadened Lines. *Reviews of Modern Physics*, **17 (2/3)**, 227–236.

- Zhang, W., 2002: FY-3 Series, The Second Generation of Polar-Orbiting Meteorological Satellites of China. Asian Conference on Remote Sensing. [Available online at <http://www.climatescience.gov/Library/sap/sap1-1/finalreport/default.htm>].
- Zou, C.-Z., , M. Gao, and M. D. Goldberg, 2009: Error Structure and Atmospheric Temperature Trends in Observations from the Microwave Sounding Unit. *Journal of Climate*, **22** (7), 1661–1681.
- Zou, C.-Z., M. D. Goldberg, Z. Cheng, N. C. Grody, J. T. Sullivan, C. Cao, and D. Tarpley, 2006: Recalibration of Microwave Sounding Unit for Climate Studies Using Simultaneous Nadir Overpasses. *Journal of Geophysical Research*, **111**, D19 114.